Polymer 50 (2009) 3022–3030

Contents lists available at ScienceDirect

Polymer

journal homepage: www.elsevier.com/locate/polymer

Halloysite nanotubes as a novel β-nucleating agent for isotactic polypropylene

Mingxian Liu, Baochun Guo*, Mingliang Du, Feng Chen, Demin Jia

Department of Polymer Materials and Engineering, South China University of Technology, Guangzhou 510640, China

ARTICLE INFO

Article history:
Received 22 August 2008
Received in revised form
13 April 2009
Accepted 22 April 2009
Available online 3 May 2009

Keywords:
Polypropylene
β-Crystal
Halloysite

ABSTRACT

The nucleating ability of halloysite nanotubes (HNTs) towards isotactic polypropylene (iPP) was investigated by differential scanning calorimetry (DSC), X-ray diffraction (XRD), polarized optical microscopy (POM) and scanning electron microscopy (SEM). HNTs are identified to have dual nucleating ability for α-iPP and β-iPP under appropriate kinetics conditions. The formation of β-iPP is dependent on the HNTs loading in the iPP/HNTs composites. The composite with 20 phr of HNTs is found to have the highest content of β-iPP. Under non-isothermal crystallization the content of β-iPP increases with decreasing of the cooling rate. The maximum β-crystal content is obtained at cooling rate of 2.5 °C/min. The supermolecular structure of the β-iPP is identified as β-hedrites with flower-cup-like and axialite-like arrangements of the lamellae. Under isothermal crystallization the β-crystal can be formed in the temperature range of 115–140 °C. Outside the temperature range, no β-iPP can be observed. The content of β-crystal reaches the maximum value at crystallization temperature of 135 °C. The formation of the β-iPP in the composites is correlated to the unique surface characteristics of the HNTs.

1. Introduction

As a semi-crystalline polymer, isotactic polypropylene (iPP) is probably one of the most interesting commodity thermoplastic widely used in many areas such as home appliances, automotive, construction, and other industrial applications, not only for its balance of physical and mechanical properties, but also due to its environmental friendliness (non-toxicity and recyclability) and low cost [1]. Recently iPP nanocomposites consisting nanosized inclusions have attracted great attentions due to their scientific and technology importance. Compared with the conventional composites of iPP, the iPP nanocomposites usually exhibited very different processibility and performance, which are tremendously affected by the crystallization of iPP matrix [2–10].

iPP is a polymorphic material with several crystal modifications including monoclinic (α), trigonal (β), and orthorhombic (γ) forms [11]. The experimental observations suggested that the α modification is thermodynamically stable. Commercial iPP crystallizes mostly in α modification under normal processing conditions and adding some α-crystal nucleating agents can enhance the clarity and reduce haze of iPP [12,13]. The β form is thermodynamically metastable and can only be obtained under some special conditions such as using temperature gradient [14,15], flow-induced crystallization [16–22] and adding special nucleating agent [23]. γ Modification is the least frequently observed, although it has been obtained after crystallizing samples at high pressures [24–26]. As the β-crystals have many performance characteristics such as improved ductility and impact strength, many research groups have focused their interest on the β-iPP. Among the techniques for preparing high content of β-iPP, adding the β-nucleating agent is the most effective and accessible method. Incorporating nanoparticles to iPP can bring the changed crystallization behavior. Generally, the nanoparticles influence the crystallization process of iPP by acting as heterogeneous nuclei. The heterogeneous nucleation leads to the increases in nucleating and crystallization rate. As a result, the increased crystallization temperature and finer spherulites are observed. On the other hand, addition of nanoparticles to iPP alters the polymorphism of iPP. Nanosized fillers such as montmorillonite (MMT) [27,28], carbon nanotubes (CNTs) [29], silica [30], magnesium hydroxide [31], calcium carbonate [32], zinc oxide [33], aluminum oxide [34], rare earth [35] etc. have been reported to have β-nucleating ability. However, the β-crystal content (Φ_β, calculated according the XRD result) in these composites is relatively low (not higher than 30%). In addition, the dependence of β-crystals on thermodynamic conditions for these composites has not been disclosed. Although the β-nucleating mechanism of iPP by small organic molecules has been suggested by Lotz and co-workers [36–40], the formation mechanism of β-iPP in the PP/inorganics systems has not been elucidated.

Halloysite nanotubes (HNTs) modified polymer composites have raised researcher's interest in the recent years due to their unique structures and properties [41–46]. HNTs, with molecular formula of $Al_2Si_2O_5(OH)_4 \cdot nH_2O$ are naturally occurred multi-walled inorganic nanotubes which have a similar geometry of CNTs. HNTs from

* Corresponding author. Fax: +86 20 2223 6688.
E-mail address: psbcguo@scut.edu.cn (B. Guo).

0032-3861/$ – see front matter © 2009 Elsevier Ltd. All rights reserved.
doi:10.1016/j.polymer.2009.04.052

different regions vary in dimension and the typical size of halloysite is 300–1500 nm in length, 40–120 nm for the outer diameter and 15–100 nm for the inner diameter. The HNTs were reported to have high mechanical strength and modulus. They are considered as the ideal materials for preparing polymer composites due to the following facts: (i) HNTs are rigid materials and with a higher aspect ratio; (ii) comparing with other nanoparticles such as fumed silica, montmorillonite, and carbon nanotubes, HNTs are more easily dispersed in polymer matrix by shearing due to the following two facts. Geometrically, the rod-like geometry of HNTs is easily dispersed due to the limited intertubular contact area. Chemically, HNTs are recognized as with relative low hydroxyl density on the HNTs outer surfaces compared with fumed silica and other layered silicates such as montmorillonite [44]. Therefore, the aggregation induced by the intertubular hydrogen bonding is susceptible to the shearing force. In fact, morphology study for many polymer/HNTs composites has shown single-tube dispersed HNTs in the matrix [42,47,48].; (iii) HNTs are cheap, abundantly available and biocompatible [49]. HNTs incorporated polymer composites show promising properties especially for the largely increased mechanical performance. For example, the storage modulus of the epoxy/HNTs hybrid with 12 wt% HNTs is 58.6% higher at 50 °C and 121.7% higher at 210 °C than that of the neat epoxy [42]. Polypropylene/HNTs and rubber/HNTs composites also show about 50% increased modulus by 30 phr HNTs than those for the neat polymers and the increase is consistent with the Halpin–Tsai model [44,48,50]. In the present paper, we compound the HNTs with iPP for preparing the iPP/HNTs nanocomposites. The influence of the HNTs on the crystallization of iPP was investigated in detail. The β-crystal of iPP induced by HNTs was firstly reported and the nucleating mechanism was suggested. The present work presents a controllable approach to obtain high level β-iPP in the iPP/inorganics composites.

2. Experimental

2.1. Materials

The isotactic iPP, with a melt flow index of 2.84 g/10 min (after ISO-1133: 1997(E)), was purchased from Lanzhou Petro-chemical Co., China. The HNTs were mined from Yichang, Hubei, China and were purified according to the reference [51]. The elemental composition of HNTs by X-ray fluorescence (XRF) was determined as follows (wt.-%): SiO_2, 58.91; Al_2O_3, 40.41; Fe_2O_3, 0.275; TiO_2, 0.071. The Brunauer–Emmett–Teller (BET) surface area of the used HNTs was 50.4 m^2/g [42].

2.2. Preparation of iPP/HNTs nanocomposites

A two-screw extruder was used to prepare the iPP/HNTs nanocomposites. The temperature setting of extruder from the hopper to the die was 180/190/195/200/200/190 °C, and the screw speed was 100 rpm. The pelletized granules were dried for 5 h under 80 °C and then injection molded under the temperature of 200 °C. The contents of HNTs in the recipes are weight parts per 100 part iPP.

2.3. Characterization of the iPP/HNTs nanocomposites

2.3.1. Differential scanning calorimetry (DSC)

DSC data of all samples were measured by a TA Q20 using nitrogen as purging gas. The samples were heated to 210 °C at the ramping rate of 40 °C/min. The sample was kept at 210 °C for 5 min to eliminate the thermal history before it was cooled down to 40 °C at the rate of 10 °C/min. The second endothermic and exothermic flows were recorded as a function of temperature.

To study the formation of β-iPP during non-isothermal crystallization, the neat iPP and iPP/HNTs composite (100/20, weight ratio) were selected to conduct the following DSC measurements. The samples were heated from ambient temperature to 210 °C at the heating rate of 40 °C/min and the temperature was hold at 210 °C for 5 min to eliminate the thermal history. Then the samples were cooled to ambient temperature at the constant cooling rates of 2.5 °C/min, 5 °C/min, 10 °C/min, 20 °C/min, and 40 °C/min. Finally, they were heated to 210 °C at the heating rate of 10 °C/min. The crystallization and melting curves were recorded.

The percentage of β-crystal, Φ_β, can be obtained from the crystallinities of the α-crystal and β-crystal according to Ref. [52]

$$\Phi_\beta(\%) = \frac{X_\beta}{X_\alpha + X_\beta} \times 100 \tag{1}$$

$$X_i(\%) = \frac{\Delta H_i}{\Delta H_{i\theta}} \times 100 \tag{2}$$

where X_α and X_β are the crystallinities of the α- and β-crystal, respectively, which can be calculated separately according to Eq. (2), where ΔH_i is the calibrated specific fusion heat of either the α- and the β-form, ΔH_i^θ is the standard fusion heat of the α- and β-crystals of iPP, being 178 J/g and 170 J/g, respectively [53]. Because the DSC curves of some samples exhibit both α- and β-crystal, the fusions were determined according to the following calibration method [54]. A vertical line was drawn through the minimum between the α- and β-fusion peaks and the total fusion heat was divided into β-component, ΔH_β^*, and α-component, ΔH_α^*. Since the less-perfect α-crystals melt before the maximum point during heating and contributed to the ΔH_β^*, the true value of β-fusion heat, ΔH_β^*, has approximated by a production of multiplying ΔH_β^* with a calibration factor A.

$$\Delta H_\beta = A \times \Delta H_\beta^* \tag{3}$$

$$A = \left[1 - \frac{h_2}{h_1}\right]^{0.6} \tag{4}$$

$$\Delta H_\alpha = \Delta H - \Delta H_\beta \tag{5}$$

h_1 and h_2 are the heights from the base line to the β-fusion peak and minimum point respectively (Fig. 1). Although the calibration method was applied, this method for determining the β-iPP content

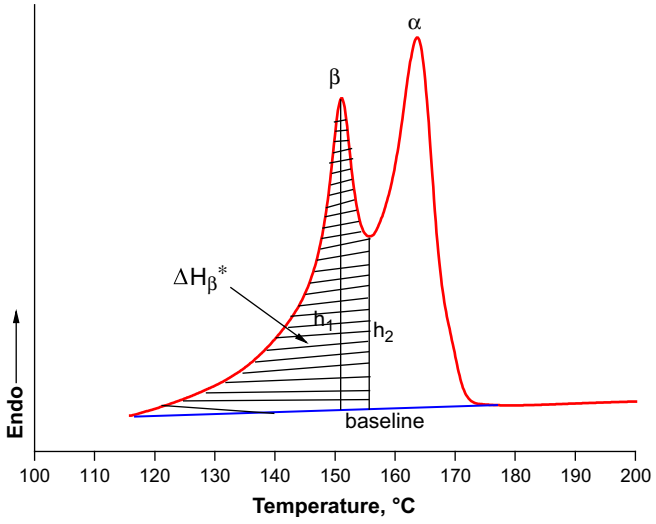

Fig. 1. DSC melting curves of iPP containing β-crystal.

was an approximate method and the obtained Φ_β value was not equal to the real value.

To study the formation of β-iPP during isothermal crystallization, the iPP/HNTs composite (100/20, weight ratio) was heated from ambient temperature to 210 °C at the heating rate of 40 °C/min and then quickly cooled to the crystallization temperature of 115 °C, 120 °C, 130 °C, 135 °C, 140 °C and 145 °C at a rate of 60 °C/min. The samples were crystallized at the crystallization temperature for 120 min and then quickly cooled to 40 °C at cooling rate of 60 °C/min. Finally, the samples were heated to 210 °C at the heating rate of 10 °C/min. The second melting curves were recorded.

2.3.2. X-ray diffraction (XRD)

The XRD patterns were recorded using the PANalytical X'pert PRO X-RAY Diffractometer. The CuKα radiation source was operated at 40 kV power and 40 mA current. Patterns were recorded by monitoring those diffractions that appeared from 5° to 40°. The scanning speed was 1°/min. The XRD samples were prepared by DSC TAQ 20 under the same conditions described above. The relative content of β-crystal, K_β, was calculated according to Equation (6) suggested by Turner-Jones [55]:

$$K_\beta = I_{\beta1}/\left(I_{\beta1} + I_{\alpha1} + I_{\alpha2} + I_{\alpha3}\right) \quad (6)$$

where $I_{\beta1}$ is the diffraction intensity of β (300) planes at diffraction angle $2\theta = 16°$, $I_{\alpha1}$, $I_{\alpha2}$ and $I_{\alpha3}$ are the diffraction intensities of the α (110), α (040), and α (130) planes at diffraction angles $2\theta = 14.1°$, 16.9° and 18.8° respectively. For all the XRD profiles, the amorphous background was extracted and then the peaks were deconvoluted with the X'Pert HighScore Plus software. After that the diffraction intensity for the reflection peaks are obtained. It should be noted that the K_β value obtained by this method was recognized as a relative measure of the proportion of β-crystal, since it included in the calculation only selected peaks instead of the entire collection of diffractions.

2.3.3. Polarized optical microscopy (POM)

The morphologies of the crystallites of the composites were recorded with an Olympus BX41 polarized optical microscopy with a Linkam hot stage. The extruded samples were placed between two microscopy slides, melted and pressed at 210 °C for 5 min to remove any trace of crystal. The morphology of the neat iPP and the composites were recorded to give the information for dispersion of HNTs in the melt. Then the composite samples (with 20 phr HNTs) were cooled to ambient temperature at the constant cooling rates of 2.5 °C/min, 5 °C/min, 10 °C/min, 20 °C/min, 40 °C/min and the final morphology of the crystallites were recorded.

2.3.4. Scanning electron microscopy (SEM)

The SEM micrographs were taken using LEO1530 VP SEM machine. The iPP/HNTs composites (100/20, weight ratio) samples were firstly heated to 210 °C and kept for 10 min and then cooled to room temperature at the cooling rate of 2.5 °C/min. Then the sample was immerged in a permanganate solution to etch the amorphous iPP [56]. The specimen was coated with a very thin layer of gold before SEM observation.

3. Results and discussion

3.1. DSC analysis for the iPP/HNTs nanocomposites

Fig. 2(a) shows the crystallization curves of the iPP/HNTs nanocomposites with different HNTs content. It is clear that the crystallization peaks of iPP shift to higher temperature with HNTs content. The observed effects can be attributed to the nucleating effect of

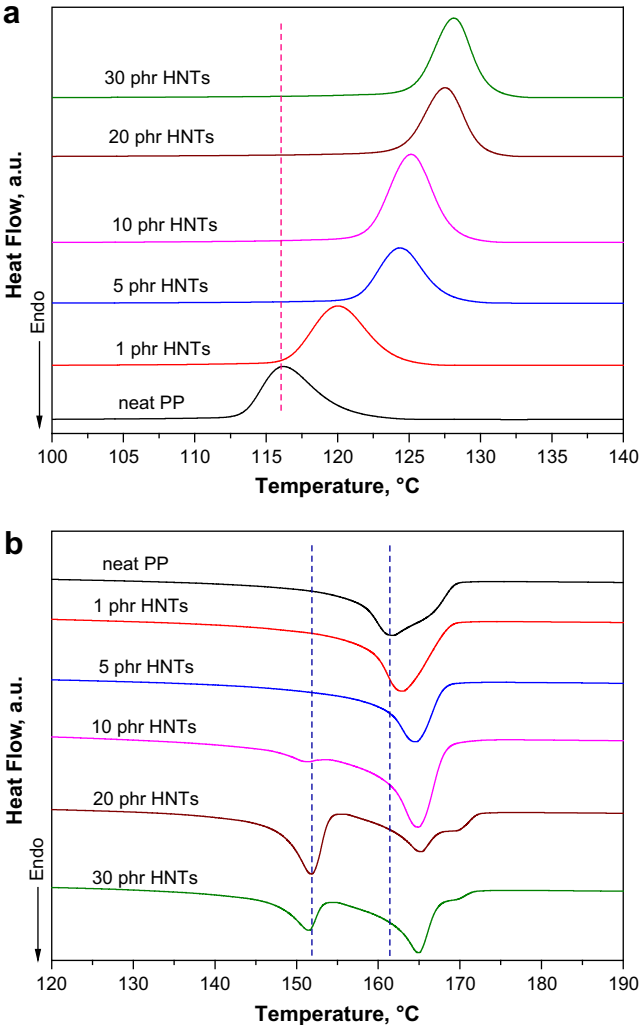

Fig. 2. DSC exothermic (a) and endothermic (b) curves of neat iPP and iPP/HNTs nanocomposites.

HNTs in iPP crystallization process. Overloading of HNTs (30 phr) in composite, however, does not provide further increase in the crystallization peak temperature. The crystallization temperature of the composites with 30 phr HNTs is nearly not changed comparing with that of with 20 phr HNTs. The over loaded HNTs may aggregate in iPP matrix and the aggregated HNTs have lower nucleating ability due to the reduced specific surface area. Similar results of the effect of HNTs in the polyvinyl alcohol (PVA) matrix have also been suggested [57]. Fig. 2(b) shows the melting curves for the iPP/HNTs nanocomposites. The peaks around 165 °C and 155 °C can be attributed to the melting of the α-crystal and β-crystal of iPP respectively [58]. The endothermic shoulder peak around 170 °C for the composite with relative high HNTs contents (above 20 phr) could be attributed to the melting of interphase between HNTs and iPP. Similar phenomena has also been reported in other composite systems such as PP/CNTs and PA/CNTs composites [59–61]. Incorporating HNTs to iPP leads to the increased melting temperature of the α-iPP although the increasing trend is not obvious at overloading (30 phr). When the HNTs loading is higher than 10 phr, the fusion of the β-iPP is observed. This phenomenon indicates the HNTs have the dual nucleating ability both for α-iPP and β-iPP. According to Equations (1)–(5), the percentage of β-crystal (Φ_β) can be calculated and the results are summarized in Table 1. Generally, the higher the content of nucleating agent is, the higher the proportion of β-crystal is. However,

Table 1
DSC data of the iPP/HNTs composites with variable HNTs content.

HNTs content (phr)	ΔH_β^* (J/g)	ΔH_β (J/g)	ΔH (J/g)	ΔH_α (J/g)	X_β (%)	X_α (%)	X_{all} (%)	Φ_β (%)
0	–	–	–	66.42	–	37.3	37.3	0
1	–	–	–	67.35	–	38.2	38.2	0
5	–	–	–	71.23	–	42.0	42.0	0
10	13.93	3.51	65.89	62.38	2.3	38.6	40.8	5.6
20	34.01	33.06	61.96	28.90	23.3	19.5	42.8	54.5
30	23.07	18.67	62.20	43.53	13.2	29.4	42.5	31.0

from Table 1, the β-crystal form content does not increase constantly. The maximum value is obtained at 20 phr of HNTs, while overloading of HNTs leads to lowered β-crystal content. This may also be attributed to the more aggregated HNTs in the composites as evidenced by the below POM result. Similar results were also reported in other β-iPP nucleating agent systems [31,62,63]. Noticeably, the total crystallinity (X_{all}) of iPP in the composites, calculated from the fusion heat in DSC result, is higher than that of neat iPP which is attributed to the heterogeneous nuclei effect of HNTs.

To investigate the dispersion of HNTs in the iPP matrix, the POM photos of iPP/HNTs nanocomposites were taken under cross-polarized light in the iPP melt and shown in Fig. 3. The morphology of HNTs in the melted iPP can be clearly observed in these photos. The dispersion of HNTs in iPP is uniform when the HNTs content is low. With increasing the content of HNTs, the aggregation of HNTs in iPP can be observed and the size of the aggregates increases gradually. When HNTs content is higher than 20 phr, the size of the HNTs aggregates is as large as 20 μm. Such big aggregates may lose

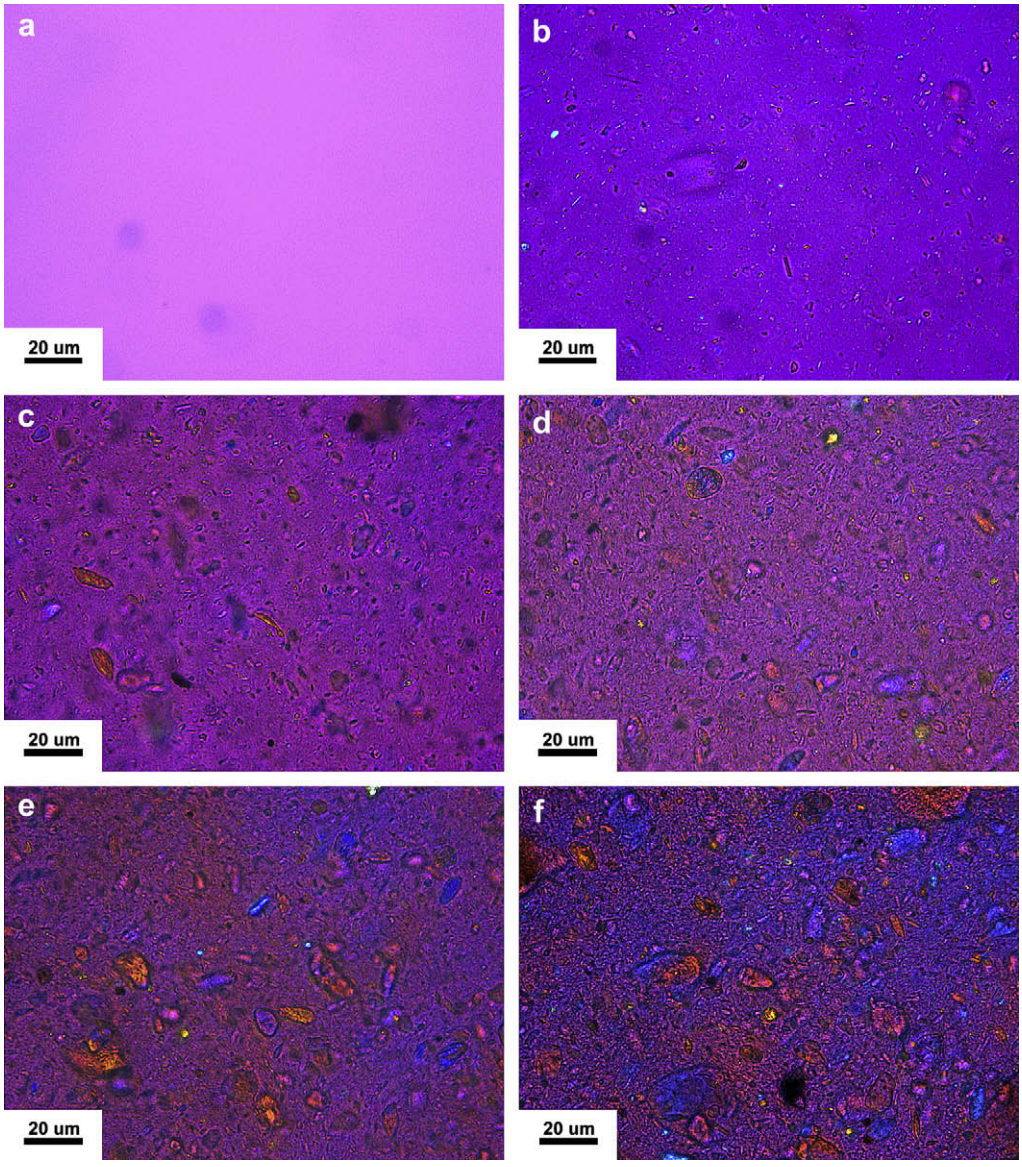

Fig. 3. POM photos of the melts of iPP and the composites with variable HNTs content (a) 0, (b) 1 phr, (c) 5 phr, (d) 10 phr, (e) 20 phr and (f) 30 phr.

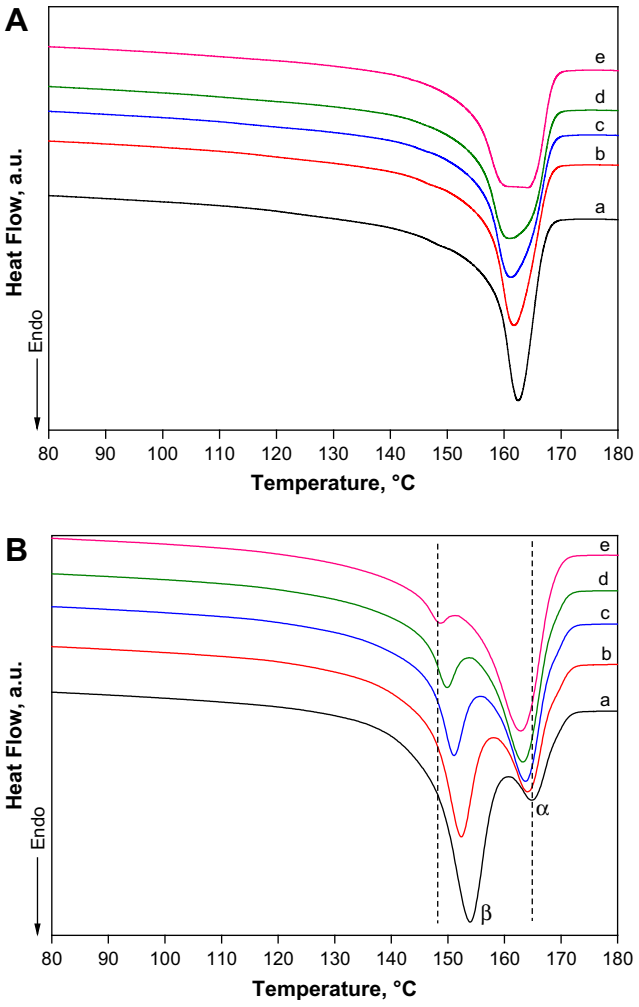

Fig. 4. DSC melting curves of neat iPP (A) and the composites (B, 20 phr of HNTs) samples non-isothermally crystallized at different cooling rate: (a) 2.5 °C/min; (b) 5 °C/min; (c) 10 °C/min; (d) 20 °C/min; (e) 40 °C/min.

their β-nucleating efficiency [63]. Therefore, the changing in Φ_β can be correlated to the dispersion change of HNTs in the matrix.

3.2. Formation of β-crystals in non-isothermal crystallization process

DSC analysis was performed to investigate the formation of β-crystals during non-isothermal crystallization with variable cooling rate. As described above the composite with 20 phr of HNTs may yield the highest content of β-crystals during non-isothermal crystallization, it is therefore selected for further study. Fig. 4(A) shows the melting curves of the neat iPP which is non-isothermally crystallized under variable cooling rate. It is clear that the crystal form of iPP is independent on the cooling rate of the non-isothermal crystallization. In absence of HNTs, all the iPP samples crystallize in the form of α-crystal. This indicates the neat iPP does not have the β-crystal nucleating ability. In the presence of HNTs, as shown in Fig. 4(B), two melting peaks, characterizing α-crystal and β-crystal, are observed in all the melting curves, suggesting dual nucleation ability of HNTs for the iPP. It is evident that the melting peak for β-crystals is consistently enlarged with decreasing cooling rate of non-isothermal crystallization, while the content of α-crystal is consistently decreased. The maximum β-crystal percentage detected by DSC reaches 64.3% at the cooling rate of 2.5 °C/min, which is

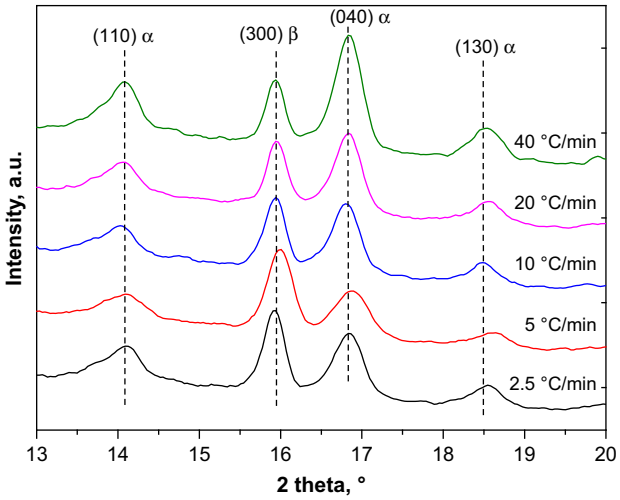

Fig. 5. XRD profiles of iPP/HNTs composite samples (20 phr of HNTs) non-isothermally crystallized at variable cooling rate.

considerably higher than that of previously reported iPP/inorganics systems [6,30,31,33,64]. When the cooling is slower, the sample will stay in the high temperature regime longer. The high crystallization temperature leads to increase in β-crystal content since the growth rate of β-crystal is considerably faster than that of α-crystal in the range of 105–140 °C [38,65–67]. The present result is consistent with that of iPP nucleated by dicyclohexylterephthalamide [68]. However, our result is contradictory with the work done by Gradys et al., in which higher cooling rate led to the increased content of β-crystal in the quinacridone-pigment Remafin Rot E3B (Hoechst) nucleated iPP. Their explanations on their results were based on the relationship between thermal stability for the different crystals form of iPP and the crystallization temperature [69]. Noticeably, the melting peak temperatures of both α-crystal and β-crystal in the composites are consistently shifted to higher temperatures when the cooling rate is decreased. This may attributed to the increased perfection of the crystals when the crystallization is conducted at lower cooling rate [70–72].

The formation of β-iPP under above non-isothermal crystallization is also substantiated by XRD experiments. Fig. 5 shows the XRD patterns of the iPP/HNTs nanocomposites non-isothermally

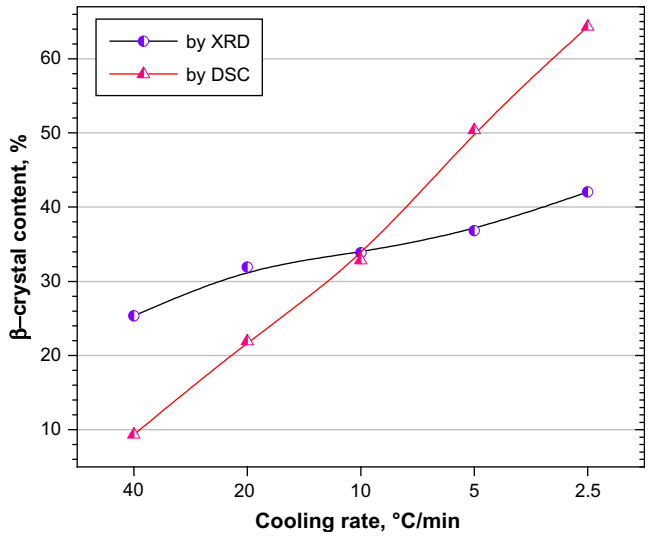

Fig. 6. Dependence of relative β-crystal content on the cooling rate.

crystallized with different cooling rates. The peaks at diffraction angles 2θ of 14.1°, 16°, 16.9°, and 18.8° are attributed to α (110), β (300), α (040), and α (130) planes respectively. Consistent with the results from DSC, β-iPP diffraction peaks are observed for all the samples. According to Equation (6), the relative content of β-crystal (K_β) is calculated. The K_β and combined with the Φ_β calculated by DSC data are plotted in Fig. 6 as a function of cooling rate. It can be seen the increasing trend of K_β with decreasing cooling rate is consistent with that for Φ_β from DSC method, although the absolute value is incomparable which is raised from different calculating theory. It should be emphasized that compared with XRD method the DSC analysis is less reliable due to the possible overlap of the melting peaks for α- and β-crystal in DSC curves.

POM was a visual method for observing the morphology of different crystals and it was employed in the present study. α- and β-crystal forms of iPP are easily distinguished under polarized light microscopy, in view of their different optical properties [37,73,74]. β-iPP spherulites are highly birefringent as a result of conventional spherulite architecture, with radiating lamellae and tangential orientation of the molecular stems in the lamellae. However, α-iPP spherulites usually are weaker birefringent as a result of a specific mechanism of lamellar branching. Therefore, in the optical micrographs, β-iPP spherulites are brighter than α-iPP spherulites [58,75,76]. Fig. 7 shows the POM morphology of iPP/HNTs composite samples (with 20 phr of HNTs) which are non-isothermally crystallized at different cooling rates. In the iPP/HNTs composite a large number of nuclei are introduced by HNTs. The nucleation rate is fast and the spherulites growth on them is a heterogeneous nucleation. Owing to large number of nuclei, the growth of spherulite is suppressed as a result of collision of the spherulites. Consequently, as shown in Fig. 7, very fine crystals with blurry boundary are observed. The cyan color parts in these photos are the bright region which indicates the presence of β-crystal of iPP. With the decrease of the cooling rate, the number of the cyan color parts in the composites increase and the area enlarges. This can be explained by the fact that the content of β-iPP in the sample crystallized at lower cooling rate is higher than that crystallized at higher cooling rate, which is consistent with the above XRD and DSC results.

The existence of β-crystals in the composite was also observed by SEM. Different types and features of supermolecular structure of

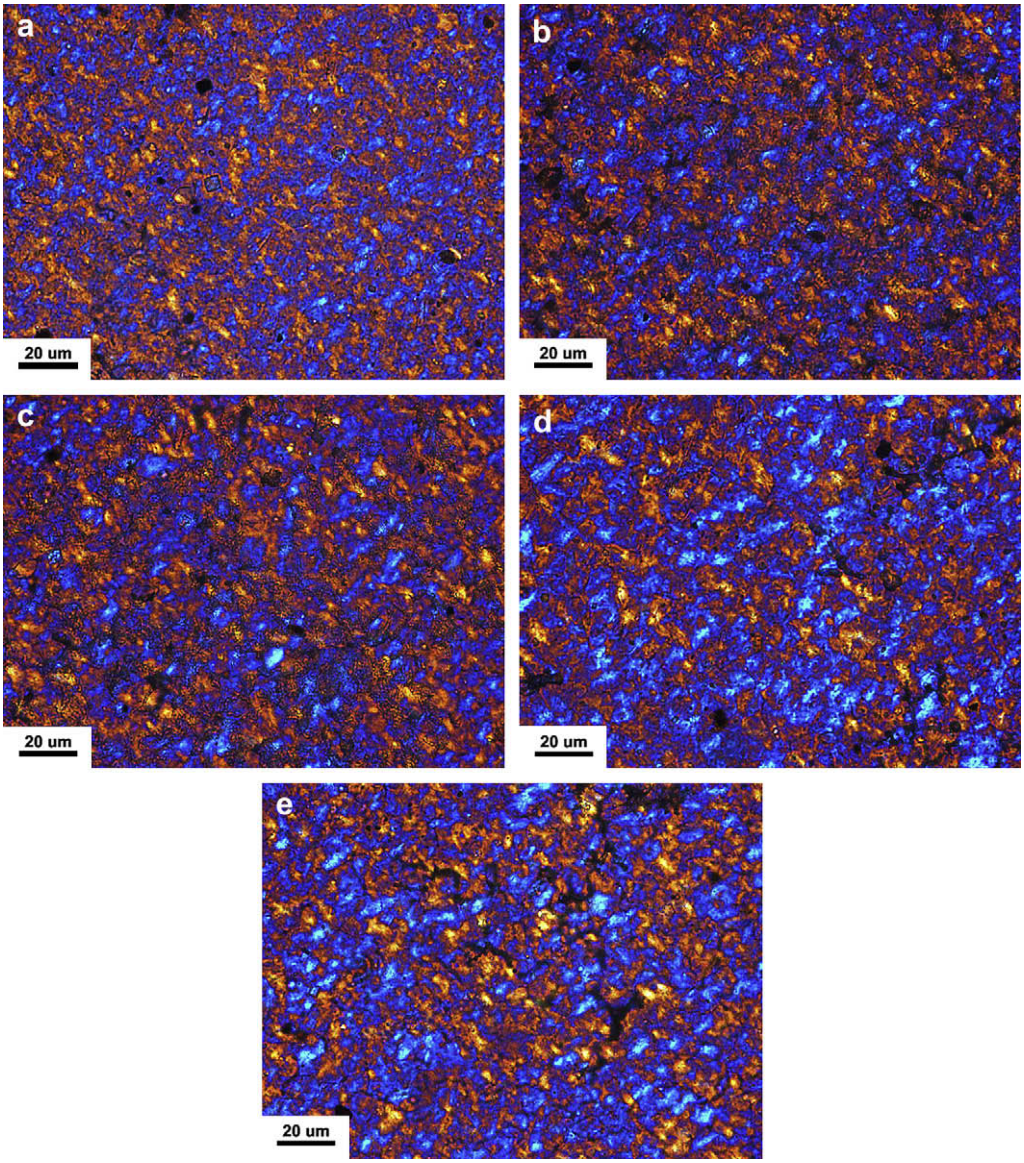

Fig. 7. POM photos of the iPP/HNTs composite samples non-isothermally crystallized at variable cooling rate: (a) 40 °C/min; (b) 20 °C/min; (c) 10 °C/min; (d) 5 °C/min; (e) 2.5 °C/min.

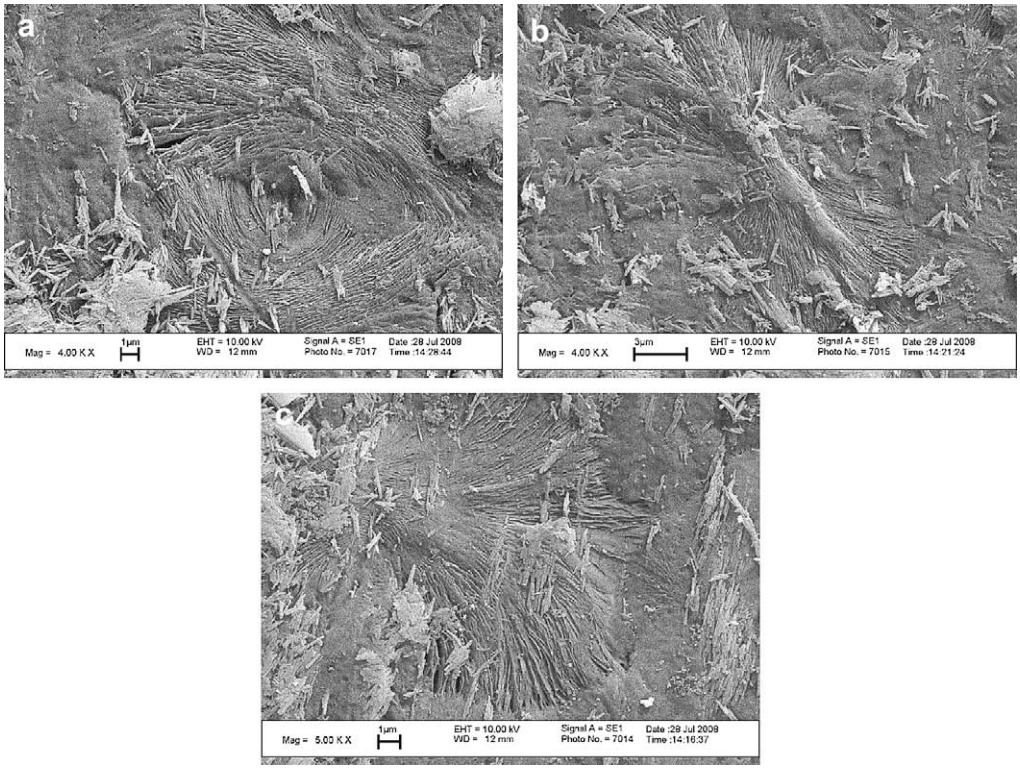

Fig. 8. SEM photos of supermolecular structure of β-crystals in the iPP/HNTs composite: (a) flower-cup-like arrangement of lamellae (b) and (c) axialite-like arrangement of lamellae.

β-iPP can be formed which are influenced by the thermal conditions of crystallization, by the melt history, by mechanical stress to the crystallizing system, and by the presence of extraneous materials. Varga has reviewed morphology features of the various supermolecular formations of β-iPP [23]. Depending on the crystallization conditions and nucleating agent, different types of the supermolecular structure of β-iPP, such as β-spherulite, β-hedrites, β-cylindrites, transcrystalline, epitaxial crystallization and single crystal-like crystalline, can be obtained. Fig. 8 shows the morphology of the etched composite sample in which the amorphous PP is essentially removed. The sheaf-like β-iPP lamellae which are curved and twisted can easily be identified under SEM [56,77]. Both flower-cup-like (Fig. 8a) and axialite-like arrangements of lamellae (Fig. 8b and c) which are subtypes of the β-hedrites are observed in the samples. Noticeably, HNTs and their aggregates are also observed in the samples which are relatively white parts in the SEM photos, as they are inert to the permanganate solution.

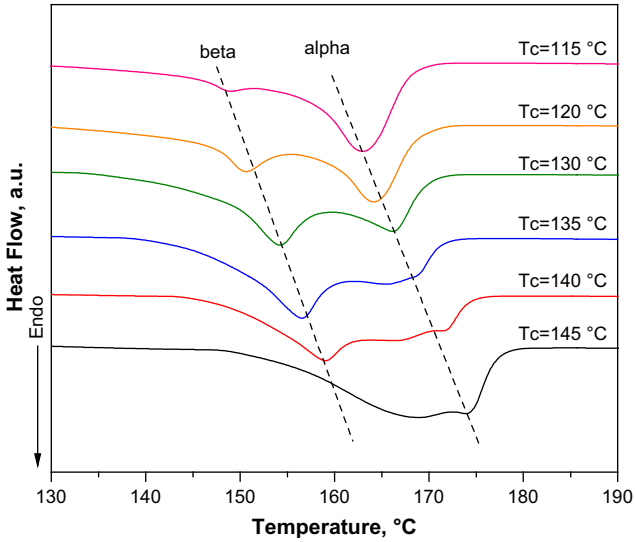

Fig. 9. DSC melting curves of iPP/HNTs composite samples (20 phr HNTs) crystallized at the variable temperature.

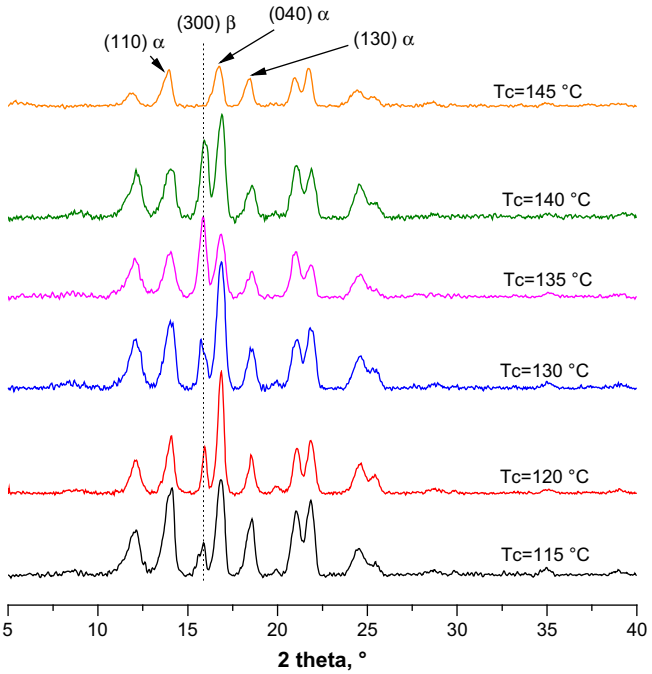

Fig. 10. XRD profiles of iPP/HNTs composite samples (20 phr HNTs) crystallized at the variable temperature.

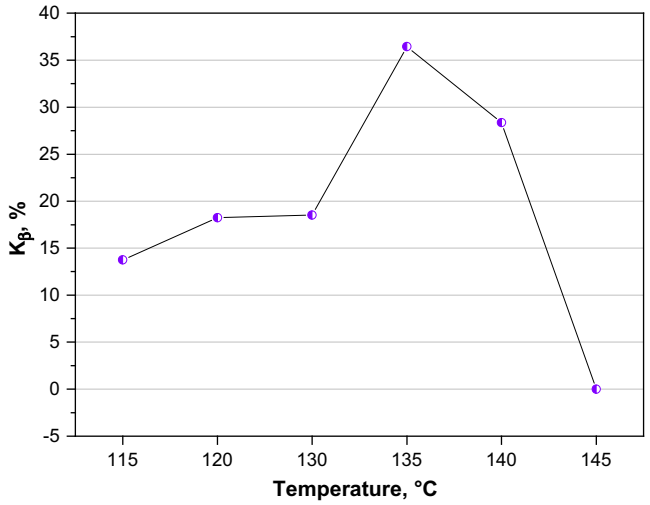

Fig. 11. Dependence of relative content of β-crystal (K_β) in the iPP/HNTs composite samples (20 phr HNTs) on the isothermal crystallization temperature.

3.3. Formation of β-crystals in isothermal crystallization process

Crystallization temperature has great influences on the β-crystal nucleating ability of the nucleating agent, which in turn will influence the phase structure of the iPP. Many works have been done on investigating the influence of the crystallization temperature on the final crystal structure in the β-nucleated iPP [62,68,78]. Fig. 9 shows the DSC melting curves of the composite samples isothermally crystallized from melt at different temperatures. It is clear that the β-crystal can be obtained in a certain temperature range (from 115 °C to 140 °C) although its accurate content is hardly calculated owing to highly overlap of β-crystal melting and α-crystal melting. When the crystallization temperature is higher than 140 °C, no β-crystal melting peak can be observed. This result is consistent with some reported systems [62,63,68]. Su et al. have attributed to this phenomenon to the result of two competing kinetic and thermodynamic effects [62]. In the range of 100–140 °C the linear growth rate of the β-crystal is greater than that of α-crystal. Outside the temperature range, the growth rate of α-iPP is higher than that of β-iPP [79]. As a result, no β-crystal melting is observed for the composite sample crystallized at 145 °C. In addition, the melting temperatures of both α-iPP and β-iPP increase with increasing crystallization temperature. This may be explained according to the kinetic theory of crystallization [65].

To further verify the influence of the crystallization temperature on the crystal forms of iPP, XRD experiment was performed on the composite samples. Fig. 10 shows the XRD profiles of the composite samples crystallized at different temperatures. It can be seen a diffraction peak at 15.9° assigning to β (300) is observed in all the samples, except the sample crystallized at 145 °C. This is consistent with the DSC result. The calculated K_β value from the XRD profiles was plotted in Fig. 11. It is clear that the increasing crystallization temperature of the composites leads to the increase in the content of β-crystal in the temperature range of 115–135 °C. The content of β-crystal in the composites reaches the maximum value of 36.4% at the crystallization temperature of 135 °C. Although the content of β-crystal for the sample crystallized at 140 °C is higher than that for 115 °C, 120 °C, and 130 °C, it starts to decrease and eventually disappears when the crystallization temperature is 145 °C. This result again confirms the upper limit temperature for β-iPP nucleation.

3.4. β-Crystal nucleation mechanism of HNTs for iPP

Understanding the nucleation mechanism of β-nucleating agent is both scientifically and technologically significant. However, the nucleation mechanism of the β-iPP for nucleating agent is still not well understood. The "dimensional lattice matching theory" proposed by Lotz et al. have been widely accepted for some β-nucleating agents of iPP [22,36–39,80], although it is not applicable to all β-nucleating agents [62]. In the theory, Lotz et al. explained the β-iPP nucleating ability through analyzing the structure relationship between nucleating agent and the β-iPP. A lattice matching between *c*-axis periodicity of iPP (6.5 Å) and a corresponding distance in the substrate crystal face of nucleating agent is the main reason for inducing the β-iPP polymorph. The nucleating agents provide the nucleation surfaces for iPP crystal. HNTs have unique morphology among other common nanoparticles such as nanosilica and other clay such as MMT. They are multi-walled inorganic nanotubes and rolled

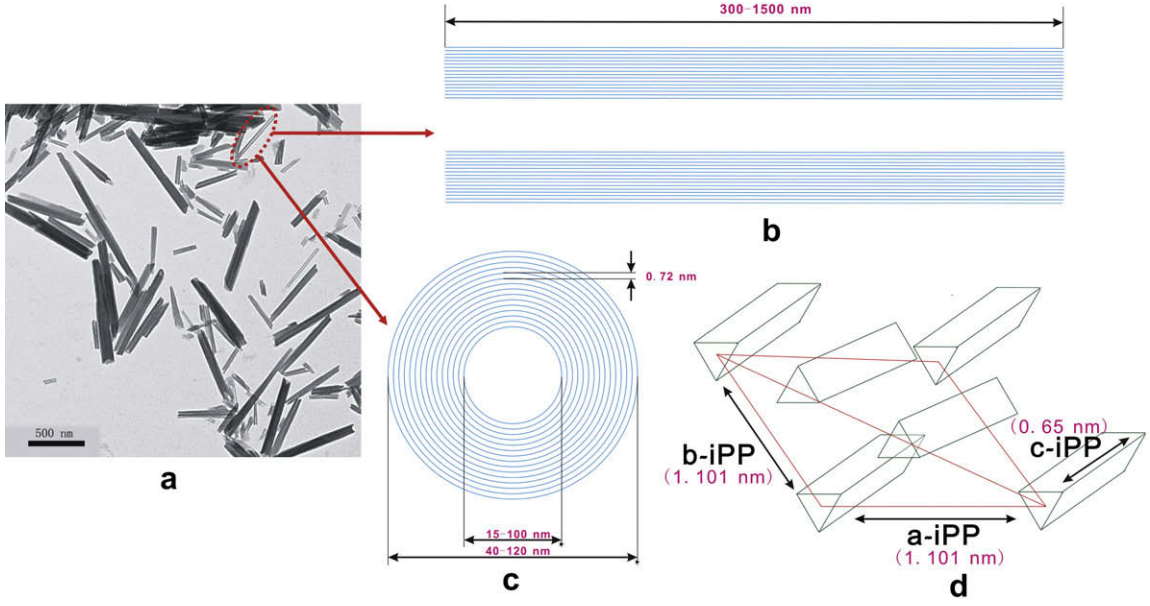

Fig. 12. TEM photos of the HNTs (a) and schematic of the crystalline structure of HNTs (b) and (c) and β-iPP (d).

by 15–20 aluminoslicate layers. The XRD diffraction spectra of HNTs (not shown) indicate a layer spacing of 0.73 nm [41]. The morphology of HNTs, the structure parameters of the HNTs, and the cell parameters of β-iPP [37,81] are depicted in Fig. 12. It can be seen the length of *c*-axis corresponding to the period of the 3_1 helix of iPP is 0.65 nm, while the layer spacing of HNTs is 0.73 nm. These two values are fairly close. Kawai et al. proposed the equation of misfit factor (f_m) between the two crystal structures of iPP and the nucleating agent which can be calculated as

$$f_m = \frac{PB - PA}{PA} \times 100 \quad (7)$$

where PA and PB are the appropriate period length of substrate and polymer respectively [82]. If $f_m < 15\%$, the epitaxy is regarded good. The f_m between the layer spacing of HNTs and the *c*-axis of iPP is 10.96%, indicating good epitaxy. For the present systems, both the outer surface and the ends of HNTs may provide the nucleation surfaces for iPP crystal. Particularly, the defects on the surfaces with appropriate size and the ends of HNTs may provide numerous nucleation surfaces when they are close to the dimension of the *c*-axis of PP. Therefore, it should be believed that the ability of HNTs inducing the nucleation of β-iPP is related to its unique microstructure and surface properties. The composites with high HNTs content (above 10 phr) provided enough sites for the nucleation and development of the β-iPP crystal and this leads to the formation of high β-iPP content under appropriate kinetics conditions.

4. Conclusions

HNTs are identified to have dual nucleating ability for α-iPP and β-iPP under non-isothermal and isothermal crystallization. The formation of β-iPP is dependent on the HNTs loading in the iPP/HNTs composites. The composite with 20 phr of HNTs is found to have the highest content of β-iPP. Under non-isothermal crystallization the content of β-iPP increases with the decrease in the cooling rate. The maximum β-crystal content is obtained at cooling rate of 2.5 °C/min. The supermolecular structure of the β-iPP is identified as β-hedrites with flower-cup-like and axialite-like arrangements of the lamellae. Under isothermal crystallization the β-crystal can be formed in the temperature range of 115–140 °C. Outside the temperature range, no β-iPP can be observed. The content of β-crystal reaches the maximum value at crystallization temperature of 135 °C. The formation of the β-iPP in the composites is correlated to the unique surface characteristics of the HNTs.

Acknowledgments

We are grateful for the financial support by the National Natural Science Foundation of China with grant number of 50603005 and the Doctorate Foundation of South China University of Technology.

References

[1] Pasquini N, Addeo Antonio. Polypropylene handbook. 2nd ed. Hanser Gardner Publications; 2005.
[2] Maiti P, Nam PH, Okamoto M, Hasegawa N, Usuki A. Macromolecules 2002; 35:2042.
[3] Lozano K, Barrera EV. J Appl Polym Sci 2001;79:125.
[4] Asuka K, Liu BP, Terano M, Nitta KH. Macromol Rapid Commun 2006;27:910.
[5] Chen JH, Chiou YD. J Polym Sci Part B Polym Phys 2006;44:2122.
[6] Labour T, Gauthier C, Seguela R, Vigier G, Bomal Y, Orange G. Polymer 2001; 42:7127.
[7] Song SJ, Wu PY, Feng JC, Ye MX, Yang YL. Polymer 2009;50:286.
[8] Vanegas ME, Quijada R, Serafini D. Polymer 2009. doi:10.1016/j.polymer.2009.03.006.
[9] Bailly M, Kontopoulou M. Polymer 2009. doi:10.1016/j.polymer.2009.03.034.
[10] Lonkar SP, Morlat-Therias S, Caperaa N, Leroux F, Gardette JL, Singh RP. Polymer 2009;50:1505.
[11] Lotz B, Wittmann JC, Lovinger AJ. Polymer 1996;37:4979.
[12] Bernland K, Tervoort T, Smith P. Polymer 2009. doi:10.1016/j.polymer.2009.03.010.
[13] Housmans J-W, Gahleitner M, Peters GWM, Meijer HEH. Polymer 2009. doi:10.1016/j.polymer.2009.02.050.
[14] Fujiwara Y. Colloid Polym Sci 1975;253:273.
[15] Lovinger AJ, Chua JO, Gryte CC. J Polym Sci Polym Phys Ed 1977;15:641.
[16] Jay F, Haudin JM, Monasse B. J Mater Sci 1999;34:2089.
[17] Varga J. Angew Makromol Chem 1983;112:191.
[18] Varga J, Karger-Kocsis J. Polym Bull 1993;30:105.
[19] Varga J, Karger-Kocsis J. J Polym Sci Part B Polym Phys 1996;34:657.
[20] Varga J, Karger-Kocsis J. J Mater Sci Lett 1994;13:1069.
[21] Kalay G, Bevis MJ. J Polym Sci Part B Polym Phys 1997;35:265.
[22] Huo H, Jiang SC, An LJ. Macromolecules 2004;37:2478.
[23] Varga J. J Macromol Sci Phys 2002;41:1121.
[24] Campbell RA, Phillips PJ, Lin JS. Polymer 1993;34:4809.
[25] Meille SV, Phillips PJ, Mezghani K, Bruckner S. Macromolecules 1996;29:795.
[26] Bruckner S, Phillips PJ, Mezghani K, Meille SV. Macromol Rapid Commun 1997;18:1.
[27] Medellin-Rodriguez FJ, Mata-Padilla JM, Hsiao BS, Waldo-Mendoza MA, Ramirez-Vargas E, Sanchez-Valdes S. Polym Eng Sci 2007;47:1889.
[28] Ding C, He H, Guo BC, Jia DM. Polym Compos 2008;29:698.
[29] Grady BP, Pompeo F, Shambaugh RL, Resasco DE. J Phys Chem B 2002; 106:5852.
[30] Jain S, Goossens H, van Duin M, Lemstra P. Polymer 2005;46:8805.
[31] Shen H, Wang YH, Mai KC. Thermochim Acta 2007;457:27.
[32] Zhang QX, Yu ZZ, Xie XL, Mai YW. Polymer 2004;45:5985.
[33] Zhao H, Li RKY. Polymer 2006;47:3207.
[34] Zhao H, Li RKY. J Polym Sci Part B 2005;43:3652.
[35] Feng JC, Chen MC, Huang ZT, Guo YQ, Hu HQ. J Appl Polym Sci 2002;85:1742.
[36] Wittmann JC, Lotz B. Prog Polym Sci 1990;15:909.
[37] Lotz B. Polymer 1998;39:4561.
[38] Stocker W, Schumacher M, Graff S, Thierry A, Wittmann JC, Lotz B. Macromolecules 1998;31:807.
[39] Mathieu C, Thierry A, Wittmann JC, Lotz B. Polymer 2000;41:7241.
[40] Mathieu C, Thierry A, Wittmann JC, Lotz B. J Polym Sci Part B Polym Phys 2002;40:2504.
[41] Du ML, Guo BC, Jia DM. Eur Polym J 2006;42:1362.
[42] Liu MX, Guo BC, Du ML, Cai XJ, Jia DM. Nanotechnology 2007;18:455703.
[43] Ning NY, Yin QJ, Luo F, Zhang Q, Du RN, Fu Q. Polymer 2007;48:7374.
[44] Liu MX, Guo BC, Zou QL, Du ML, Jia DM. Nanotechnology 2008;19:205709.
[45] Ye YP, Chen HB, Wu JS, Ye L. Polymer 2007;48:6426.
[46] Mu B, Zhao MF, Liu P. J Nanopart Res 2008;10:831.
[47] Liu MX, Guo BC, Lei YD, Du ML, Jia DM. Appl Surf Sci 2009;255:4961.
[48] Du ML, Guo BC, Lei YD, Liu MX, Jia DM. Polymer 2008;49:4871.
[49] Lvov YM, Shchukin DG, Mohwald H, Price RR. ACS Nano 2008;2:814.
[50] Du, ML. PhD dissertation. South China University of Technology, 2007.
[51] Shchukin DG, Sukhorukov GB, Price RR, Lvov YM. Small 2005;1:510.
[52] Shangguan YG, Song YH, Peng M, Li BP, Zheng Q. Eur Polym J 2005;41:1766.
[53] Li JX, Cheung WL, Jia DM. Polymer 1999;40:1219.
[54] Li JX, Cheung WL. Polymer 1998;39:6935.
[55] Turner-Jones A, Alizlewood JM, Beckett DR. Macromol Chem 1964;75:134.
[56] Xu W, Martin DC, Arruda EM. Polymer 2005;46:455.
[57] Liu M, Guo B, Du M, Jia D. Appl Phys A 2007;88:391.
[58] Padden FJ, Keith HD. J Appl Phys 1959;30:1479.
[59] Brosse AC, Tence-Girault S, Piccione PM, Leibler L. Polymer 2008;49:4680.
[60] Phang IY, Ma JH, Shen L, Liu TX, Zhang WD. Polym Int 2006;55:71.
[61] Saeed K, Park SY. J Appl Polym Sci 2007;106:3729.
[62] Su ZQ, Dong M, Guo ZX, Yu J. Macromolecules 2007;40:4217.
[63] Zhao SC, Cai Z, Xin Z. Polymer 2008;49:2745.
[64] Supaphol P, Thanomkiat P, Junkasem J, Dangtungee R. Polym Test 2007;26:20.
[65] Varga J. In: Karger-Kocsis J, editor. Poly(propylene): structure, blends and composites, Vol. 1. London: Chapman & Hall; 1995. p. 56–115 [chapter 3].
[66] Lotz B, Fillon A, Thierry A, Wittmann JC. Polym Bull 1991;25:101.
[67] Sun X, Li H, Wang J, Yan S. Macromolecules 2006;39:8720.
[68] Zhang YF. J Polym Sci Part B Polym Phys 2008;46:911.
[69] Gradys A, Sajkiewicz P, Minakov AA, Adamovsky S, Schick C, Hashimoto T, et al. Mater Sci Eng A 2005;413:442.
[70] Di Lorenzom ML, Silvestre C. Prog Polym Sci 1999;24:917.
[71] Xu WB, Ge ML, He PS. J Polym Sci Part B Polym Phys 2002;40:408.
[72] Supaphol P. J Appl Polym Sci 2000;78:338.
[73] Bruckner S, Meille SV. Nature (London) 1989;340:455.
[74] Boucher E, Flolers JP, Creton C, Hervet H, Leger L. Macromolecules 1997; 30:2102.
[75] Norton DR, Keller A. Polymer 1985;26:704.
[76] Varga J. J Mater Sci 1992;27:2557.
[77] Li JX, Cheung WL, Chan CM. Polymer 1999;40:2089.
[78] Varga J, Menyhard A. Macromolecules 2007;40:2422.
[79] Li H, Sun X, Yan S, Schultz JM. Macromolecules 2008;41:5062.
[80] Yamaguchi M, Fukui T, Okamoto K, Sasaki S, Uchiyama Y, Ueoka C. Polymer 2009;50:1497.
[81] Lu QL, Dou Q. e-Polymers 2008. Article number: 076.
[82] Kawai T, Iijima R, Yamamoto Y, Kimura T. Polymer 2002;43:7301.